Analysis of high-speed Al-PLIF images to study aluminum droplet combustion in solid propellant flames

Pier-Henri Chevalier, Robin Devillers, Nelly Dorval, Gautier Vilmart, Brigitte Attal-Trétout, Christophe Brossard, Xavier Mercier, Julien Pichillou

Analysis of high-speed Al-PLIF images to study aluminum droplet combustion in solid propellant flames

Pier-Henri Chevalier, Robin Devillers, Nelly Dorval, Gautier Vilmart, Brigitte Attal-Trétout, Christophe Brossard, Xavier Mercier, Julien Pichillou

DOI: 10.13009/EUCASS2019-605

Analysis of high-speed Al-PLIF images to study aluminum droplet combustion in solid propellant flames

Pier-Henri Chevalier[*], *Robin Devillers*[**], *Nelly Dorval*[*], *Gautier Vilmart*[*], *Brigitte Attal-Trétout**, *Christophe Brossard*[*], *Xavier Mercier*[***], *Julien Pichillou*[****]

[*]*DPHY, ONERA, Université Paris-Saclay, F-91123 Palaiseau, France*
pier-henri.chevalier@onera.fr; nelly.dorval@onera.fr; gautier.vilmart@onera.fr;christophe.brossard@onera.fr
brigitte.attal-tretout@onera.fr
[**] *DMPE, ONERA, Université Paris-Saclay, F-91123 Palaiseau, France*
robin.devillers@onera.fr;
[***]*Lille University, CNRS, UMR 8522 – PC2A,F-59000 Lille France;*
xavier.mercier@univ-lille.fr
[****] *CNES, the Launcher Directorate, 52 Rue Jacques Hillairet – 75612 Paris Cedex France ;*
julien.pichillou@cnes.fr

Abstract

The combustion of aluminum particles is a key factor for solid-propellant propulsion in terms of performance and stability. An automatic detection of droplets in Al-PLIF image was developed. The "Maximally Stable Extremal Regions" detection method is evaluated on two image sets previously obtained at 1.0 and 1.5 MPa. The method shows good detection performances compared to a set of Ground Truth images for both pressure levels. When applied to 3000-image series, more than 35000 objects were detected on LIF images. This is very promising for future statistical analysis of Al combustion based on Al-PLIF diagnostic.

1. Introduction

Solid propulsion is commonly used for space and military applications such as launcher Ariane V or MICA and AASM missiles. For typical applications, solid propellants are mixed with amonium perchlorate (AP) into a polymer binder such as hydroxyl-terminated polybutadiene (HTPB) and additives components. Flows inside a solid propellant motor are most of the time multiphase. Aluminum combustion is highly exothermic and is used to increase flame temperature and so improves specific impulse. The weight fractions can be up to 20%. However, aluminum particles are carried away in the motor flows and combustion begins close to the propellant surface. Those phenomena can lead to dramatic impacts including performance instabilities [1][2][3] or solid-phase losses, which justifies the need for experimental and numerical studies. Various approaches have been taken in order to model the aluminum combustion in rocket booster configurations, such as using flame diffusion theory studies of hydrocarbon droplets combustion or resolving kinetic and transport equations of each gas species around an isolated droplet [4][5][6][7]. The combustion behavior is also strongly dependent on the size of particles. In order to obtain reliable experimental data, non-intrusive techniques have to be used, with combustion conditions as close as possible to solid-propellant motor operating conditions.

Development of planar laser-induced fluorescence of aluminum atoms (Al-PLIF) including spectroscopic studies was carried out earlier in steady-state conditions inside two dedicated evaporation chambers [8]. Both systems were used in order to validate the excitation/detection scheme (309/394-396 nm) and to quantify the pressure and saturation effects on signal behavior. A theoretical model including quenching and saturation effects was elaborated and validated through a number of experiments among which fluorescence decay time measurements. The method was validated in solid-propellant flames with pressure up to 1.2 MPa [10]. It showed a high potential to enable more precise analysis of aluminum combustion with both LIF and emission signals. It is important to specify that, in those experiments, images were recorded with a repetition rate of 10 kHz. Due to the high amount of images (approximatively 20,000) recorded during the combustion time of propellant samples (around 2 seconds), as well as the presence of several particles in each image, automatic algorithms would be useful to expand the previous combustion analysis targeting a group of droplet trajectories to get more statistically-relevant populations.. Analysis

DOI: 10.13009/EUCASS2019-605

of previous shadowgraphy images obtained earlier in our lab had highlighted the potential of the Maximally-Stable Extremely Regions algorithm (MSER [11]) for particle detection [12]. Results were found to be promising and suggested that the algorithm could be applied to PLIF images. The purpose of this paper is to describe the algorithm adaptation for fluorescence-images analysis. A first analysis is presented in this study. First, the Al-PLIF diagnostic is briefly presented. Inputs and validation parameters are introduced to present a first parametric analysis on the detections. Finally, an analysis of droplet detection with MSER over a complete image set is provided and discussed.

2. Experimental apparatus and conditions

2.1 Al-PLIF principle

The recently developed Al-PLIF has been used to characterize Al droplet combustion in solid propellant ambiance [10]. The experimental setup has been described elsewhere [[10]. A quick overview is presented here. The excitation laser system is composed of a frequency doubled Nd:YAG laser (Edgewave, INNOSLAB2011-E) at 532 nm pumping a frequency doubled dye laser (Sirah Credo, Lasertechnics) emitting at 309 nm. The laser system operates with a repetition rate of 5 kHz, with a 5 ns pulse duration, and an energy per pulse of 280 µJ. The beam is shaped into a laser sheet of 17 mm in height and 150 µm in thickness thanks to a combination of UV-fused silica lenses (f = 618 mm, f = -19 mm, f = 200 mm). With this configuration, a large portion of the propellant flame is entirely covered. The repetition rate is high enough so that particle travel distances are short from one image to another, which enables their trajectories to be reconstructed. The complete experimental setup is described in Figure 1.
The laser sheet enters the combustion chamber through a UV fused silica window. The fluorescence is measured at right angle from the laser direction. Light is amplified by an UV intensifier (HS-IRO, Lavision) and acquired by a CMOS camera (12 bit, La Vision HSS6). Fluorescence light is filtered by two passband filters centered at 394 nm (FWHM = 10 nm) and one long-pass filter (cutoff wavelength = 385 nm) A field of view of same height than the laser sheet is obtained by means of a Cerco objective (94 mm) and a set of spacers (16 × 16 mm²). A resolution of 22 µm/pixel is obtained over 768 × 768 pixels area.
The acquisition frequency is set to 10 kHz (twice the laser frequency) in order to alternate successively images with and without laser excitation. The complete camera system is set on a motorized translation stage with 12.5 µm step. This stage is particularly useful to focus camera on laser sheet and solid propellant sample positions.

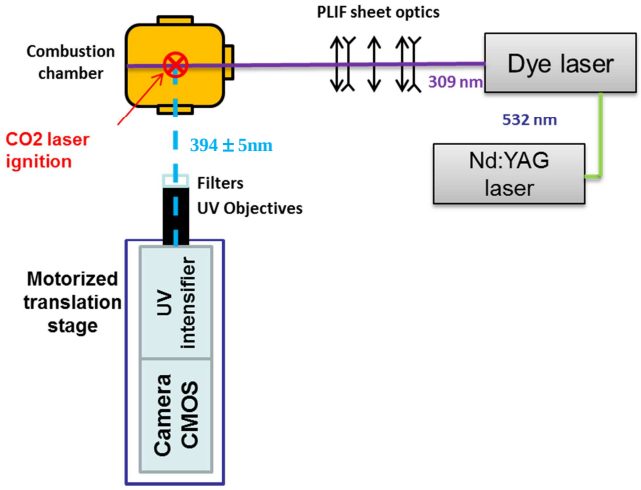

Figure 1: PLIF experimental setup implemented on the combustion chamber

An example of two consecutive images of a propellant burning at 1.5 MPa is shown in Figure 2. The first image is recorded with laser tuned to the Al absorption line [9]. The second image is recorded without laser and thus only shows emission background from the particles and the hot gases. By comparing the two images, one can distinguish the LIF signal from the emission: LIF signal is seen to be concentrated into some droplets and around those droplets (in red circles), and also a more diffuse signal spread over the plume is produced when laser in on. This latter signal is attributed to LIF signal from Al atoms by recording images with laser detuned. The droplets (in red circles) are

DOI: 10.13009/EUCASS2019-605

thus unambiguously attributed to aluminum droplets which are located within the laser sheet and composed of liquid/gaseous aluminum. In contrast, other droplets (in yellow circles) do not show important variation of signal from one image to the other, revealing no LIF signal. The droplets are either out of the laser sheet or are not composed of aluminum but are totally oxidized (Al_2O_3).

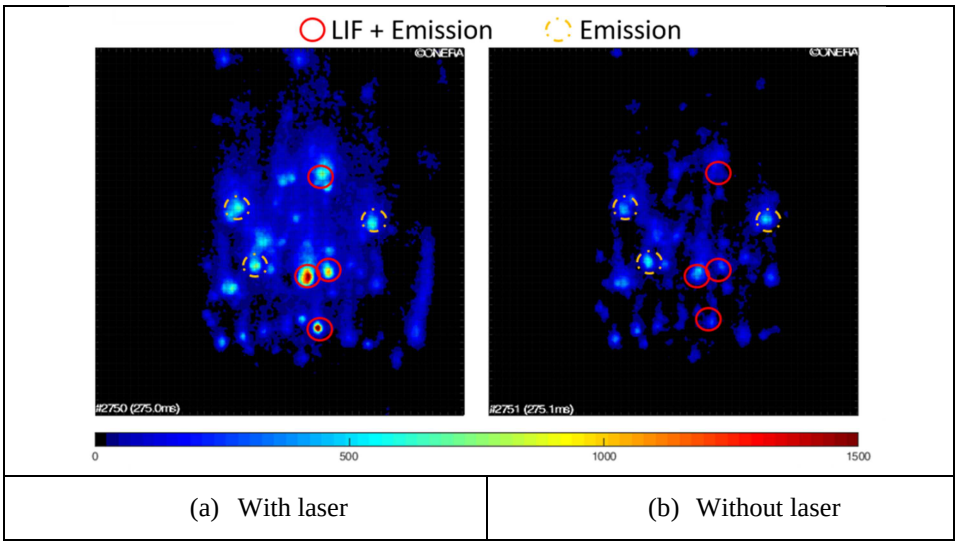

(a) With laser | (b) Without laser

Figure 2: Two consecutive images recorded during solid propellant combustion (1.5 MPa) in (a), there is laser excitation (Al-PLIF image) and in (b) there is not. Signal dynamic is set to 1500 counts.

2.2 Solid-propellant composition and burning conditions

Various tests have been carried out on a solid-propellant research composition made of Al, AP particles, embedded in a HTPB binder. The aluminum weight fraction is 18%. The combustion chamber is pressurized with nitrogen at pressure from 1.0 MPa to 1.5 MPa as described previously [13]. The intensifier gate duration has been reduced below 100 ns as used previously [8,9] in order to limit the emission background contribution as much as possible, knowing that the fluorescence time decay is much shorter [9]. Two tests with gate duration set at 40 and 20 ns were used for the MSER analysis. The characteristics are referenced in the table 1. Two pressure levels were tested to study its influence on the flame, 1.0 and 1.5 MPa. Detection parameters were first adjusted on the 1.5 MPa test because this corresponds to the most difficult detection conditions.

Table 1: Test conditions for the various image series.

Diameter [µm]	Series label #	Pressure [MPa]	Intensifier gate [ns]
10 - 200	8-111	1.5	40
	8-104	1.0	20

3. Al-droplet automatic detection approaches

This section presents the automatic detection methods that were used. The approach selected for the evaluation of detection performances is described.

3.1 Used detection algorithms

The MSER method [11] was used to detect the aluminum droplet leaving the propellant surface. The basic principle is to binarize the image according to various threshold levels. The goal is to find stable regions over the tested threshold range. A region is considered stable as long as the area variation of the region does not exceed a fixed criterion denoted MaxVariation. A given object can lead to various stable regions in terms of area variations, for

DOI: 10.13009/EUCASS2019-605

instance when a small sub-region is included in a larger one. The algorithm will only extract the maximally stable regions, considered more relevant. MSER enables detection of droplets whatever their sizes with various ranges of intensity levels and independently from their overall sharpness. Such features seem to be appropriate for the targeted objects found in the present PLIF images.
The MSER input parameters are the following:

- *Delta*: controls the range of threshold over which area stability is tested;
- *MaxVariation*: absolute value for the stability criterion used to consider a region as stable;
- *MinDiversity*: controls the way the algorithm deals with various stable regions included in one another, for example regions that are stable enough (compared to MaxVariation) but are included in other stable regions with a larger dimension. The use of this parameter was found to improve detection performances.

A parametric study was conducted in order to provide good detection performances. Delta and MaxVariation can be considered as connected parameters: various pairs (Delta; MaxVariation) are able to lead to similar detections and performances. Hence it was decided to keep a fixed Delta value and only test various MaxVariation values. Additionally various MinDiversity values were tested. Detection performances were obtained by comparison to ”ground truth” images (see section 3.2). The tested intervals are referenced in the table below. The listed values correspond to input values used directly on an existing Matlab version of MSER. Normalized input values are used in this version: for instance the largest MaxVariation value is 1.0.
For the sake of comparison, the detection performances were compared to fixed threshold detections used as detection baseline. Various fixed-threshold values were tested in order to illustrate trends regarding the baseline approach.

Table 2: Range of MSER input parameters tested to adjust detection.

	Delta	**MaxVariation**	**MinDiversity**
Tested values	1	[0.1 ; 0.90]	[0.7000 ; 0.9986]
Full range	/	[0.0 ; 1.0]	[0.0000 ; 1.0000]

3.2 Ground Truth (GT) images obtained by annotations

A number of "ground truth" images (GT) was created manually to adjust detection parameters. The Al droplets were considered spherical, as observed on typical shadowgraphy images [12]. An upward plume is often observed on PLIF images as a source of PLIF signal, attributed to the presence of gaseous Al atoms in the flame surrounding the burning droplet. An example is presented in Figure 3. Two very bright circles are visible and each of them is surrounded by a larger blue area directed upward. The full areas formed by droplets with their plume were selected manually by drawing a circle around the droplet and flame and a trapeze around the plume. Two images with two different color ranges are presented in Figure 4 to illustrate the wide range of collected signal. On the left–hand side, the color scale maximum is set to 1000 counts and the largest and brightest objects are easily delimited. On the right-hand side with a maximum set to 200, droplets with a lower signal are now discernable and easier to select manually. The manual method used to generate GT images is not a foolproof method. Droplets may not have been seen by the user and can be detected by MSER (as shown in the image on the right). This may involve a non-optimal choice of detection parameters and influence the reported detection performances.

Two sets of 16 and 6 images were selected for annotations in test series # 8-111 and # 8-104, respectively. They were chosen among images obtained over the entire duration of the combustion test. The total number of annotated regions is presented in Table 3. The annotated images go in pairs. We annotated each time the PLIF image and the following emission image in order to generate statistical data for both image types. Images for test series #08-111 were used to select the MSER detection settings, which explains the larger number of images. Only 6 images were annotated for test series #8-104 because only the best MSER parameters from series #8-111 were tested. There was no MSER-parameter selection phase for test series #8-104.

Table 3. Number of Ground Truth images and targeted regions for the two analyzed series.

	8-111		**8-104**	
Category	**Images**	**Regions**	**Images**	**Regions**
PLIF	8	227	3	111
Emission	8	179	3	64

DOI: 10.13009/EUCASS2019-605

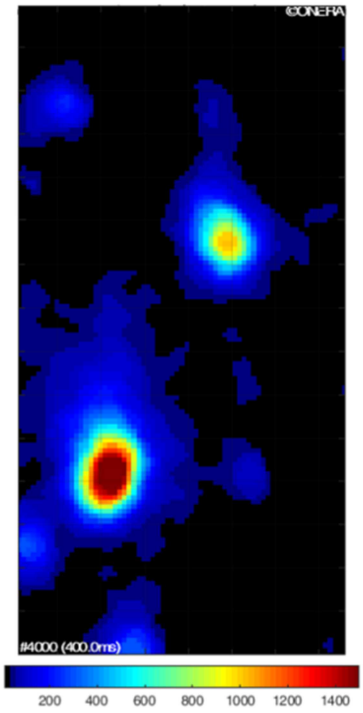

Figure 3 : Close up on some PLIF droplets for test 08-111.

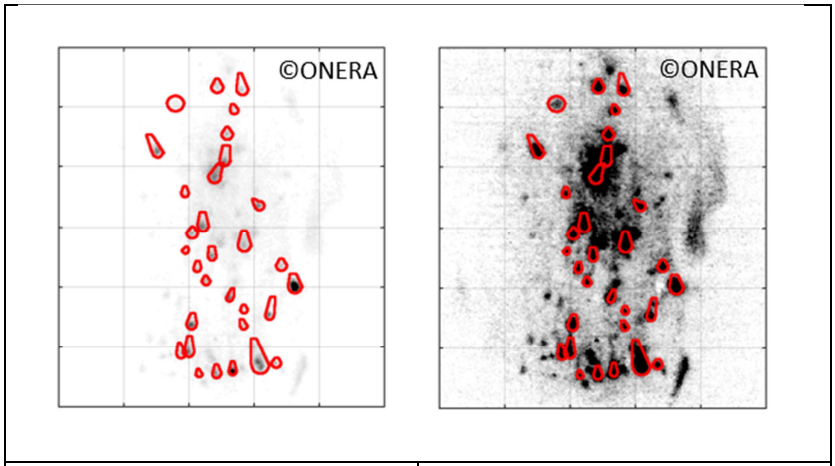

(a) Max = 1000 cnts | (b) Max = 200 cnts

Figure 4: Example of annotations selection for the same PLIF image with two different colorscale settings.

3.3 Evaluation of detection performances

Two common parameters were used to evaluate the detection performances. Comparing detection to the Ground Truth leads to three cases: True Positive (TP) represents the detection of "real" particles, False Positive (FP) represents the detection of spurious objects (noise, smoke…) and False Negative (FN) represents the real particles from the GT image not detected by the algorithm. The two quantifiers, commonly used to evaluate the detection performances, are the following [12]:

- $Recall = \frac{TP}{TP+FN}$ (1)

DOI: 10.13009/EUCASS2019-605

The Recall parameter characterizes the efficiency of the algorithm to detect a large number of real objects. A Recall parameter equals to 1 means that no real droplet from the GT was missed.

- $Precision = \frac{TP}{TP+FP}$ (2)

  The Precision parameter represents the quality of the detected objects, i.e. the algorithm capacity to avoid detecting spurious objects. For large Precision levels very few spurious detections (FP) take place.

Usually, detection performances vary with the detection parameters and are tuned according to both Precision and Recall usually plotted as Precision vs Recall. A trade-off has to be made between Precision and Recall. On one hand, Recall close to 1 (i.e. segmenting all real droplets) usually corresponds to non-strict MSER settings that also generate many false detections, i.e. lower Precision levels. On the other hand, targeting Precision values close to 1 corresponds to a very selective detection approach leading to non-detected real droplets, i.e. lower Recall levels. The effect of such a trade-off will be presented later in the article.

4. Results

This section describes the performances for Al-droplet detections obtained with MSER and the baseline detection approach for test series #8-111. It also shows MSER detections for test series #8-104 over 6 GT images. Finally MSER detections are obtained over 3000 images for each series, enabling first comments on Al-PLIF signal trends.

4.1 Baseline: detection with fixed threshold

As described earlier, a fixed threshold approach is used as detection baseline. The detection results are shown in the Figure 5 for 4 threshold levels. The number of detected droplets depends on the threshold value. On one hand, with a low threshold value, the algorithm detects the entire flame as a single area as well as many local regions mostly associated to numerical noise. On the other hand a high threshold value may not detect low intensity objects and lead to many missed objects (FN).

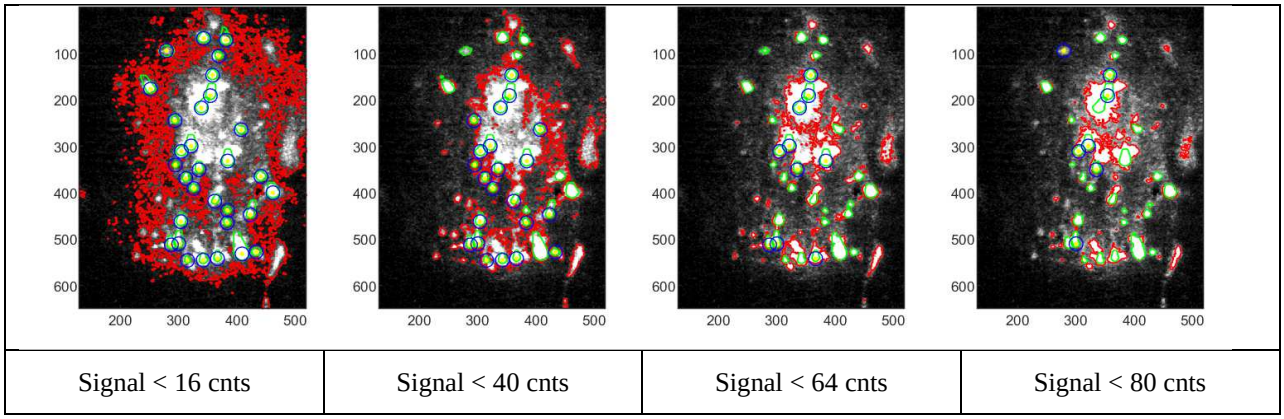

Signal < 16 cnts	Signal < 40 cnts	Signal < 64 cnts	Signal < 80 cnts

Figure 5: Results of the detection analysis with different fixed threshold levels.

Figure 6 presents a comparison between Ground Truth and fixed-threshold detections for an 80 counts threshold level. A large proportion of False Positive (red pixels) is visible around a group of droplets. Most large red areas also include green portions corresponding to the position of real droplets from the GT located within the larger detected area. However, the real droplets are not really segmented individually in this case but included into a large detected area. (one single large area is detected instead of a couple of independent droplets). Such a result is not satisfying in order to study single droplet evolution. On a brighter level, the number of False Negative pixels (in blue) remains rather low for this setting compared to the number of True Positive results.

DOI: 10.13009/EUCASS2019-605

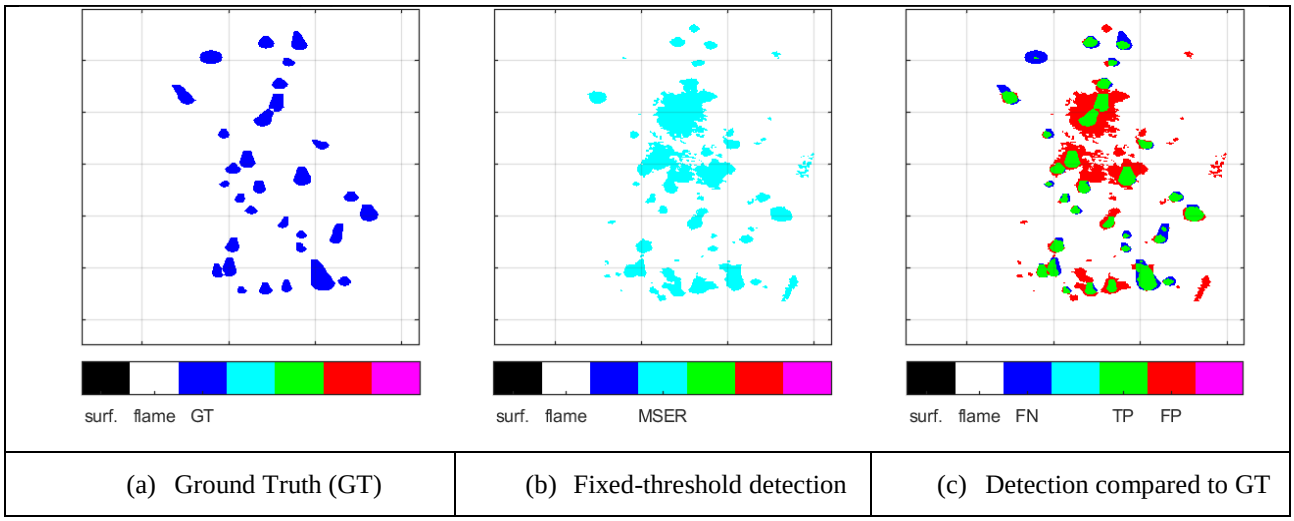

(a) Ground Truth (GT)	(b) Fixed-threshold detection	(c) Detection compared to GT

Figure 6: Comparison between Ground Truth and fixed-threshold detection (threshold level: 80).

Figure 7 presents the Precision VS Recall graph for fixed threshold detections. For threshold values between 80 and 120, the detection performances are reasonably good with both Recall and Precision close to 65%. But the proportion of False Positive remains significant. Moreover, using fixed thresholds would require adjustment for each measurement condition, which does not seem robust enough to enable analysis for various measurement series with a single detection setting.

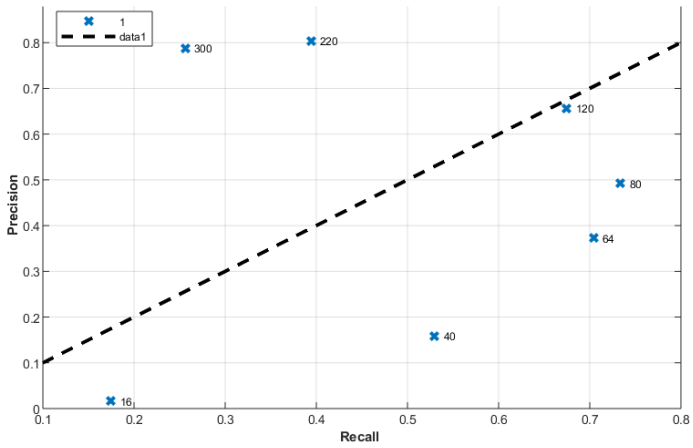

Figure 7: Detection performances for various fixed threshold levels.

4.2 Selection of MSER detection parameters

Results for the adjustment of MSER detection parameters are shown in Figure 8 with Recall and Precision levels. Precision and Recall values depend on both MaxVariation and MinDiversity. For a given MinDiversity value (i.e. along a given color curve), increasing the Recall level leads to a Precision reduction. As commented earlier, this is an expected trend for detection studies: detecting more “real droplets” usually also means detecting more spurious portions of the images. A trade-off always needs to be chosen between Recall and Precision, which can be obtained by targeting Recall and Precision values both between 0.7 and 1.0. Four settings match such a criterion and provide similar detection performances: (0.6 ; 0.9986), (0.8 ; 0.9986), (0.6 ; 0.9995) and (0.8 ; 0.9995). The pair (0.8 ; 0.9986) was chosen here for further MSER analysis.

DOI: 10.13009/EUCASS2019-605

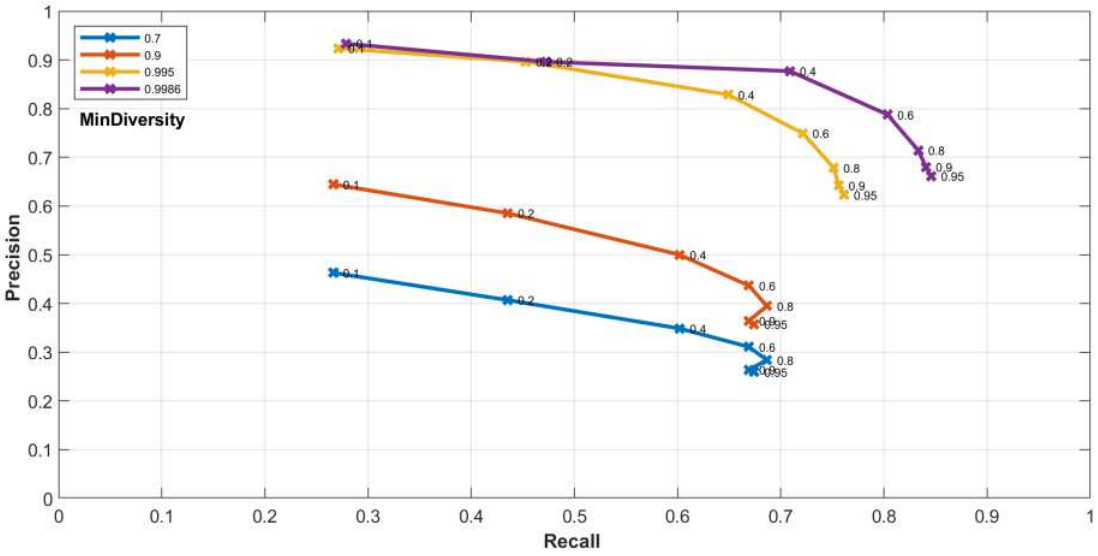

Figure 8: Detection performances for various MSER input parameters.
Each color curve corresponds to a MinDiversity value. The MaxVariation values are written next to each dot.

Figure 9 shows comparison between GT and MSER detection for 3 parameter settings for image #2500, acquired with laser excitation. Recall and Precision values for image #2500 are specified below each image. Similarly as in the case of a fixed threshold approach, the (0.995; 0.80) shows large regions with both red and green pixels. This means that the single detected region corresponds to two real GT droplets that are not detected separately. This suggests that MinDiversity needs to be larger than 0.995 in order to provide good Recall levels. The other two pairs show that increasing MinDiversity from 0.9986 to 0.999 provides a better Recall but reduces Precision, i.e. increases the number of spurious detections. This is visible with the larger number of red pixels in the comparison image for (0.999; 0.95). It is interesting to note that the results for image #2500 are better than the overall detection-performance result. This result shows the importance of evaluating detection performances for various images in order to be representative of all image conditions found over the full image series.

Detection compared to GT images	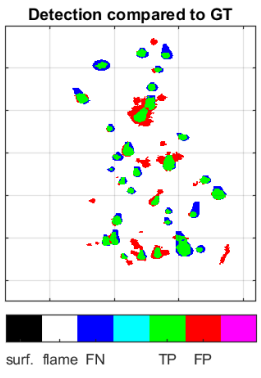	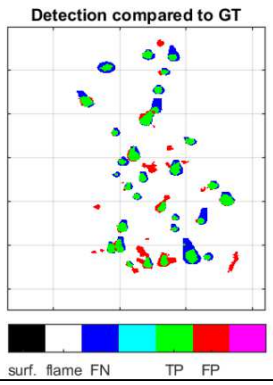	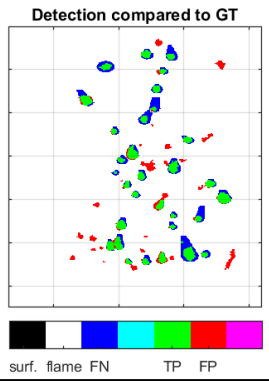
MinDiversity MaxVariation	0.995 0.8	0.9986 0.8	0.999 0.95
Performance for image #2500	Rec = 0.92 Pr = 0.70	Rec = 0.92 Pr = 0.75	Rec = 0.95 Pr = 0.57

Figure 9: Comparison of MSER detections to GT. Image #2500 with laser with reported Precision (Pr) and Recall (Rec) values for the studied image.

DOI: 10.13009/EUCASS2019-605

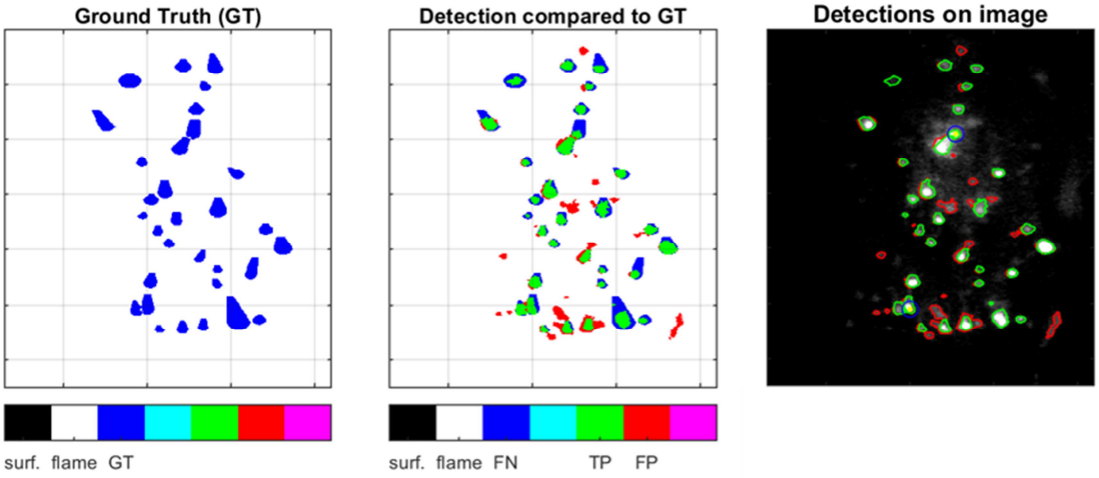

Figure 10: Comparison between Ground Truth and MSER detection with parameters (0.80 ; 0.9986)

Figure 10 shows a comparison of MSER detections with the manually annotated droplets for a PLIF image. GT and comparison between GT and MSER detections are shown on the left image and in the middle. MSER detections are overlaid on the PLIF image on the right-hand side. At first glance, not all annotated objects have been detected as seen with the two blue spots on the PLIF image. On regarding to the morphology side, various MSER detections are limited to round regions without including the full annotated flame regions (a green circle found within a larger blue region). The manually annotated surrounding flame is not particularly well detected. It seems difficult to detect both a very bright liquid droplet and the darker gas phase surrounding it with a single MSER parameter. A more specific approach might need to be investigated in the future. In addition, there are several FP (false positive) objects. This large number corresponds to a Precision level not equal to 1. But location of the FP suggests they might be real Al droplets when displayed over the PLIF image. As mentioned above, some low-contrast droplets were not annotated during constitution of GT because of their low signal level. Revisiting annotations might be required to report more accurate detection performance values but the general trends should not change.

4.3 Comparison of detection performances

The same selected MSER parameters (0.80 ; 0.9986) were applied to test series #8-104 at 1.0 MPa. The observed droplets are usually smaller and show lower signal levels. The signal level for the plume regions surrounding the detected droplets also seems less bright than in the case of the #8-111 series at 1.5 MPa. Images are shown in Figure 11 for series #8-104 both with laser excitation (on the left-hand side) and without laser excitation (on the right-hand side). The number of visible droplets in the image without laser excitation is relatively limited with the 1.0 MPa test. Less emission is visible at this lower pressure and also with a shorter intensifier gate. The MSER algorithm releases few False Positive but also misses many real droplets from the GT. On the image with laser excitation, many real droplets are detected (many green circles) and not so many objects are missed (False Negative ; not so many blue circles). This test does not mean that MSER cannot detect all the drops for test series #8-104 but that detection parameters are not optimal to detect objects on images without laser excitation when almost no emission is visible. A subsequent parametric study would certainly lead to better detection performances for this test. But using MSER parameters adjusted from another test still makes it possible here to detect LIF droplets with reasonable performances.

DOI: 10.13009/EUCASS2019-605

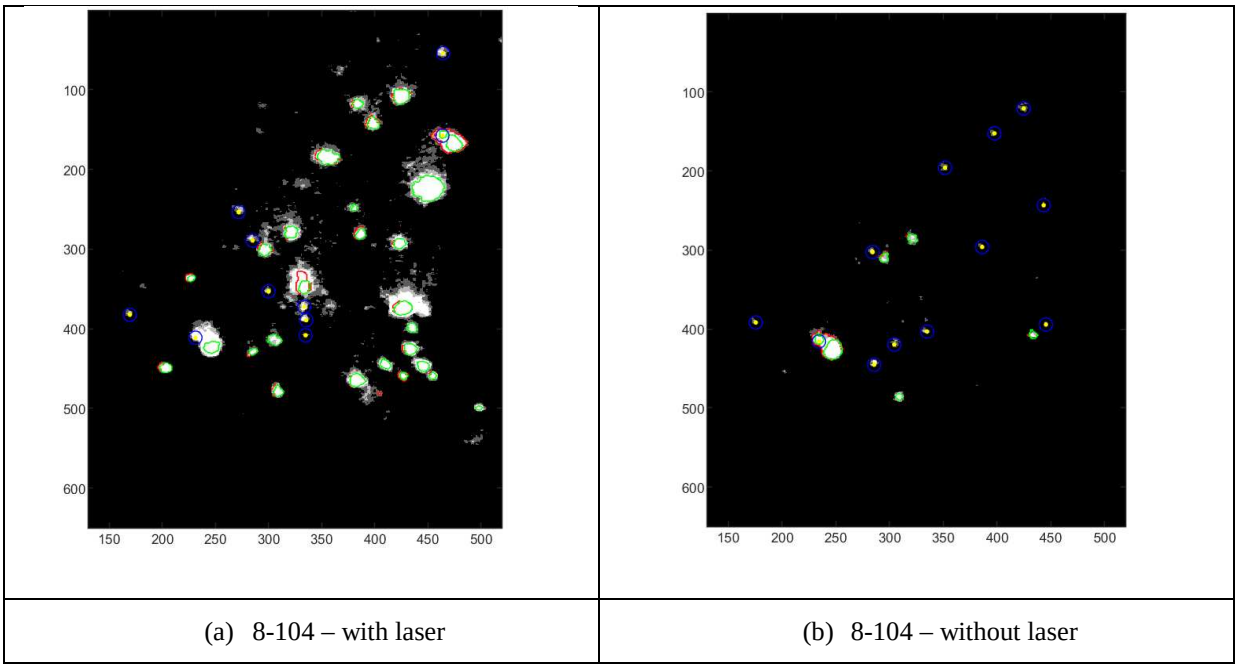

(a) 8-104 – with laser

(b) 8-104 – without laser

Figure 11 Comparison of MSER results for the 1.0 MPa test series #8-104
The MSER detection parameters are (0.80 ; 0.9986).

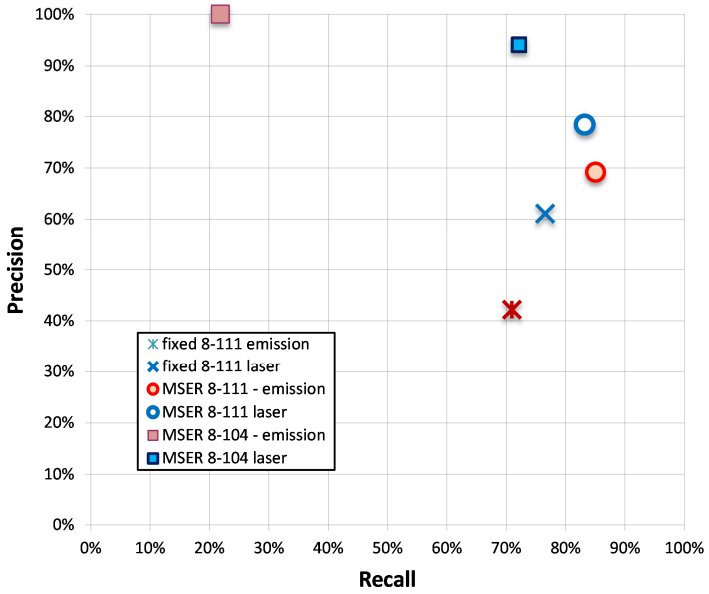

Figure 12: Precision against recall for #8-111 and #8-104 test series depending on the detection approach and the type of image (with or without laser).

Figure 12 shows detections performances for the various test conditions: #8-111 (fixed threshold and MSER), #8-104 (MSER). Performances are reported separately for images with laser and emission images. As expected, the fixed-threshold detection is less efficient than MSER for test series #8-111 both in terms of Recall and Precision. Detection performances are strongly different for the two kinds of images from series #8-104: Recall is only hardly larger than 20% for emission images. Emission was particularly low due to the reduced intensifier gate and the lower pressure conditions. As the signals are low, the algorithm has difficulty detecting objects that are barely visible to human eye on the recorded images. The chosen MSER parameters were decent but certainly non optimal for the emission

DOI: 10.13009/EUCASS2019-605

objects visible in series #8-104. Therefore, further analysis in section 5 is limited to detections for images series #8-111.

5. First analysis of detected objects performance from LIF and Emission images

MSER detection for all images for #8-111 test series was performed. The MSER settings are the one described above. The number of detections from MSER is referenced in Table 2. The number of detections on images with laser is larger than on emission-only images (without laser), similarly as in the case of the GT images. It is very interesting to see that more than 56000 objects were detected for 2000 images with laser excitation. Further analysis should provide statistically relevant data on various aspects such as signal levels, apparent diameter... With the high repetition rates, the same droplet will be detected several times on various successive images: obtaining 56000 detections do not mean that 56000 individual droplets will be studied. Tracking a given droplet will provide a much better understanding of aluminum-combustion behavior.

Table 2: Number of detected objects for test series #8-111.

Test series	**8-111 (1.5 MPa)**	
Category	*Emission only*	*With laser*
Number of detected objects	39619	56216

Figure 12 shows maximum signal distributions for the detected objects for test series #8-111at two vertical positions above the propellant surface (0.06 and 0.19). Signal levels and vertical positions have been normalized for clearer scaling. No object was detected for maximum signal levels above 0.20 to 0.25 on emission images whereas objects up to 0.73 in normalized maximum signal have been detected on images with laser excitation. The shift between the two distributions illustrate that laser excitation is able to generate high signal level compared to emission-only levels. This is very promising for future detection and analysis of Al droplets. The number of objects detected on images with laser seems to decrease slightly with the height above the propellant surface.

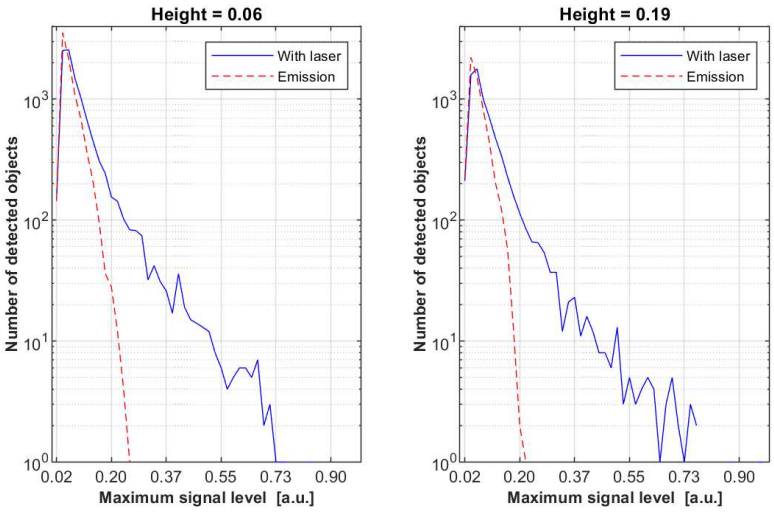

Figure 13: Signal distribution for detected objects on images with and without laser at two positions above the propellant surface for the #8-111 test.

The previous distribution was plotted for two selected heights above the propellant surface. It will be interesting to shows more precisely the influence of the distance to the propellant surface on such distributions. Figure 14 shows a 2D representation of distributions for MSER detections: as a function of maximum signal levels along the x axis and as function of the height above the propellant surface in y. Distributions from Figure 13 basically correspond to one line on the 2D distribution from Figure 14. 2D distributions are shown for images with laser and emission images for test series #8-111. The number of detections decreases with height for images with and without laser. Various phenomena can cause such decrease:

DOI: 10.13009/EUCASS2019-605

- aluminum has been consumed over vertical trajectories from the surface, leading to smaller droplets and lower signal levels ;
- alumina smokes and combustion products from the propellant are dense enough to absorb light and reduce the signal ;
  The studied flame is rather small and burns in a large volume of nitrogen initially at room temperature. A temperature drop is expected further from the propellant surface, leading to lower droplet temperatures and lower LIF and emission signals.

All this will have to be investigated in more details by studying droplet trajectories. But the results are very promising.

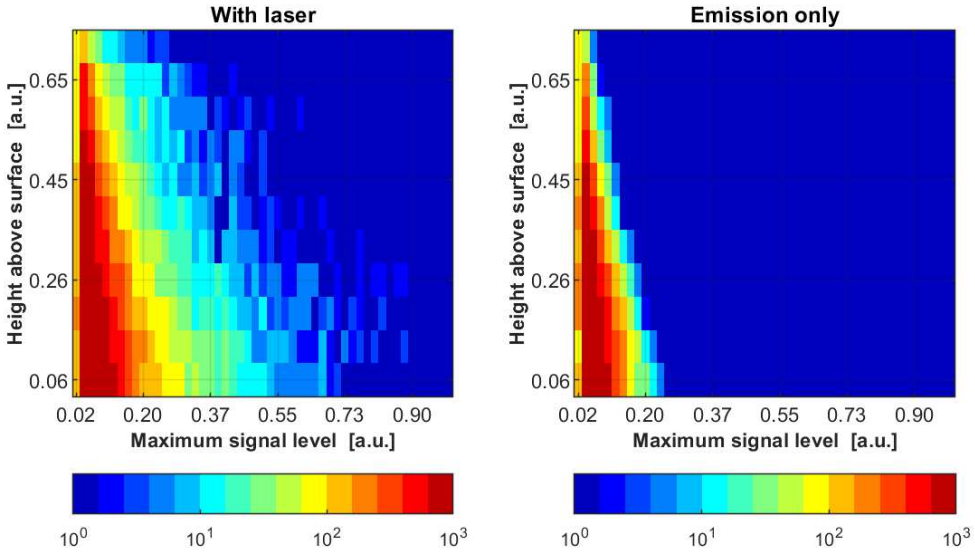

Figure 14: 2D representation of MSER detection distribution as a function of the height above the surface (vertical axis) and the maximum signal level (horizontal axis). Distribution for images with laser (on the left-hand side) and Emission (for the right-hand side) for test series #8-111.

6. Conclusion

The purpose of this paper was to propose an automated detection method for Al-particle detection in Al-PLIF images acquired during combustion in solid-propellant flames up to 1.5 MPa. Two pressure levels have been investigated, 1.0 and 1.5 MPa. The detection method used is the Maximally Stable External Regions (MSER). Annotations were made to produce a series of Ground Truth images. The images were chosen over the entire duration of the tests. A first analysis was also carried out using a fixed-threshold detection method as a baseline. It has been shown that with the fixed-threshold approach, the proportion of False Positive detection is very important. This method would require an adjustment for each test condition, which is not robust enough.

A parametric study was conducted for test series #8-111 on two MSER detection parameters (MaxVariation and MinDiversity). Precision and Recall values depend on both parameters. A trade-off must be made to obtain values between 0.7 and 1.0 for both Precision and Recall, which correspond to good detection performances. Four settings were found to satisfy the target performance range. Among them, the doublet (0.8; 0.9986) pair was chosen for all other MSER processing. Droplets with weak signals are more difficult to detect. With the same MSER detection parameter, the 1.0 MPa-test showed similar detection performance levels but only on images with laser excitation on. Since the aperture time is twice shorter for the 1.0 MPa run, the emission level is found much lower, making it too difficult to detect object on the emission image. But this is an advantage for studies targeting Al-PLIF signal.

Finally, MSER detections were obtained over 4000 images for each test series. More than 55,000 objects were detected with laser excitation on, in 1.5 MPa images. The number of detected objects with laser excitation on seems to decrease with the height above the propellant surface. This observation will have to be investigated in more details to better understand the physical phenomena involved. These results are very promising, and may provide good insight in Al-combustion behavior, especially if droplets can be followed over successive images.

DOI: 10.13009/EUCASS2019-605

Acknowledgments

This work was supported by ONERA and CNES.

References

[1] Guéry, J.F., Ballereau, S., Godfroy, F., Gallier, S., Orlandi, O., Della Pieta, P., Robert, E. & Cesco, N. 2008. Thrust Oscillations in Solid Motors. *In Proc. 44th AIAA* 2008-4979

[2] S. Gallier, F. Godfroy 2009. Aluminum Combustion Driven Instabilities in Solid Rocket Motors. *Journal of Propulsion and Power*, 25(2):509-521

[3] Casalis, G., Boyer & G., Radenac, E. 2011. Some recent advances in the instabilities occurring in long Solid Rocket Motors. *In Proc. 47th AIAA* 2011-5642.

[4] Orlandi O., Gallier S., Cesco N. 2013 Numerical simulation of a single aluminum droplet burning in a propellant environment, *5th European Conference for Aeronautics and Space Sciences (EUCASS)*

[5] Washburn E.B., Trivedi, J.N., Catoire, L., Beckstead, M.W. 2008. The simulation of the combustion of micrometer-sized aluminum particles with steam. *Combustion Science and Technology*. 180(8):1502-1517.

[6] Glorian, J., Catoire, L., Gallier, S., Cesco, N. 2015. Gas-surface thermochemistry and kinetics for aluminum particle combustion. *Proceedings of the Combustion Institute*. 35(2):2439–2446.

[7] Muller M., Davidenko D., Gianvangigli V. 2017. Computation study of aluminum droplet combustion in different atmospheres, *7th European Conference for Aeronautics and Space Sciences (EUCASS)*

[8] Vilmart, G. Détection de vapeurs d'atomes métalliques par Fluorescence Induite par Laser (LIF) : Application à la propulsion solide. Ph. D. Thesis. Université de Paris-Saclay, Orsay, 7 December 2017.

[9] Vilmart, G.; Dorval, N.; Attal-Trétout, B.; Bresson, A. 2017. Detection of iron and aluminum atomic vapors by LIF technique : application to solid propellant combustion. In Proceedings of the 33rd AIAA Aerodynamic Measurement Technology and Ground Testing Conference, Denver, Colorado, USA, 5-9 June 2017; AIAA 2017-3900.

[10] Vilmart G., Dorval N., Devillers R., Fabignon Y., Attal-Tretout B., Bresson A. 2019. Imaging aluminum particles in solid-propellant flames using LIF on Al atoms, *Materials*, in submission

[11] J. Matas, O. Chum, M. Urban, T. Pajdla Robust Wide Baseline Stereo from Maximally Stable Extremal Regions. *Proc. Of British Machine Vision Conference*, 384-396 (2002)

[12] R.W. Devillers, N. Dorval, G. Vilmart, M. Nugue, G. Le Besnerais, J. Pichillou. 2018. Aluminum particle tracking on experimental shadowgraphy and Al-PLIF images to provide velocity data for two-phase flow simulations of solid rocket motors, *Space Propulsion conference*, article #320

[13] Vilmart G., Dorval N., Orain M., Lambert D., Devillers R., Fabignon Y., Tretout B., Bresson A. .2018. Detection of iron atoms by emission spectroscopy and laser-induced fluorescence in solid propellant flames, *Applied Optics* vol. 57, No. 14, p. 3817